

See discussions, stats, and author profiles for this publication at: <https://www.researchgate.net/publication/273395489>

# High-Torque-Density Control of Multiphase Induction Motor Drives Operating Over a Wide Speed Range

Article in IEEE Transactions on Industrial Electronics · February 2015

Impact Factor: 6.5 · DOI: 10.1109/TIE.2014.2334662

---

CITATIONS

4

---

READS

74

6 authors, including:



**Michele Mengoni**

University of Bologna

59 PUBLICATIONS 407 CITATIONS

SEE PROFILE



**Luca Zarri**

University of Bologna

106 PUBLICATIONS 1,723 CITATIONS

SEE PROFILE



**Giovanni Serra**

University of Bologna

132 PUBLICATIONS 3,575 CITATIONS

SEE PROFILE

# High-Torque-Density Control of Multiphase Induction Motor Drives Operating Over a Wide Speed Range

Michele Mengoni, *Member, IEEE*, Luca Zarrì, *Senior Member, IEEE*, Angelo Tani, Leila Parsa, *Senior Member, IEEE*, Giovanni Serra, *Senior Member, IEEE*, and Domenico Casadei, *Fellow, IEEE*

**Abstract**—The high-order harmonics of the magnetic field can be used in some typologies of multiphase machine to improve the torque density. However, maximizing the torque capability depends on the thermal, voltage, and current constraints of the machine and the inverter. In this paper, a rotor-flux-oriented control scheme, which is capable of exploiting the maximum torque at any speed, is presented for multiphase induction motor drives. Below the base speed, the torque improvement is obtained by adding a third harmonic component to the fundamental component of the air-gap magnetic field. At high speeds, the amplitude of the field harmonics is progressively reduced to ensure the widest possible operating speed range. The validity of the proposed control scheme is confirmed by experimental tests.

**Index Terms**—Induction motors, multiphase drives, variable-speed drives.

## NOMENCLATURE

$N$	Number of phases.
$\rho$	Harmonic order.
$\bar{i}_{S\rho}, \bar{i}_{R\rho}$	Stator and rotor current space vectors generating the $\rho$ th spatial harmonic of the magnetic field.
$\bar{\varphi}_{S\rho}, \bar{\varphi}_{R\rho}$	Stator and rotor flux space vectors of the $\rho$ th spatial harmonic of the magnetic field.
$L_{S\rho}, L_{R\rho}$	Stator and rotor self inductances of the $\rho$ th spatial harmonic of the magnetic field.
$M_\rho$	Mutual inductance of the $\rho$ th spatial harmonic of the magnetic field.
$R_S$	Stator resistance.
$R_{R\rho}$	Rotor resistance for the current $\bar{i}_{R\rho}$ .
$\omega_m$	Rotor angular speed in electrical radians.
$i_{S1d}, i_{S1q}$	$d$ - $q$ components of the stator current vectors $\bar{i}_{S1}$

Manuscript received January 7, 2014; revised March 30, 2014 and May 25, 2014; accepted May 29, 2014. Date of publication July 2, 2014; date of current version January 7, 2015.

M. Mengoni, L. Zarrì, A. Tani, G. Serra, and D. Casadei are with the Department of Electrical, Electronic and Information Engineering “Guglielmo Marconi,” University of Bologna, 40126 Bologna, Italy (e-mail: michele.mengoni@unibo.it; luca.zarri2@unibo.it; angelo.tani@unibo.it; giovanni.serra@unibo.it; domenico.casadei@unibo.it).

L. Parsa is with the Department of Electrical, Computer, and Systems Engineering, Rensselaer Polytechnic Institute, Troy, NY 12180 USA (e-mail: parsa@ecse.rpi.edu).

Color versions of one or more of the figures in this paper are available online at <http://ieeexplore.ieee.org>.

Digital Object Identifier 10.1109/TIE.2014.2334662

$i_{S3d}, i_{S3q}$	and $\bar{i}_{S3}$ in the reference frames synchronous with $\bar{\varphi}_{R1}$ and $\bar{\varphi}_{R3}$ .
$\eta$	Ratio between the currents $i_{S3d}$ and $i_{S1d}$ .
$I_{Sd, \text{rated}}$	Nominal peak value of the sinusoidal magnetizing current of the motor.
$I_M$	Maximum admissible current.
$E_{dc}$	Voltage of the dc link.

## I. INTRODUCTION

MULTIPHASE drives, i.e., drives based on machines having more than three phases, are seen with interest in many modern applications, such as vehicle and naval propulsion systems or the more-electric aircraft [1]–[3].

In multiphase drives, in addition to the fundamental component of the magnetic field, some of the spatial harmonics can be controlled independently. This property allows reducing the amplitude of the torque pulsations (if the additional harmonics are set to zero) or improving the reliability and fault tolerance of the drive (by keeping the fundamental component of the field unchanged in case of a fault). The fault tolerance is likely the most studied feature of multiphase drives. Several fault control principles have been analyzed for permanent magnet machines and induction machines, with different numbers of phases [4]–[8].

The possibility offered by high-torque-density machines to improve the delivered torque has been of interest to researchers in the recent past. Initially, control schemes with high-torque-density capability have been proposed for permanent magnet synchronous motors [9]–[11]. Following that, some high-torque-density drives were proposed for induction motors [12], [13]. In all the initial research, the torque improvement was usually achieved by adding only the third spatial harmonic in the magnetic field under some simplifying assumptions, such as neglecting the leakage flux, and without focusing on the current and voltage constraints imposed by the inverter.

In recent years, some studies have investigated the performance of high-torque-density multiphase drives more deeply. The study in [14] presents steady-state analysis and performance evaluation of an 11-phase induction machine when harmonic injection up to the ninth harmonic or a square-wave supply is applied. For the same RMS fundamental current, the machine could be overloaded by approximately 37.5%, and the corresponding increase in the RMS phase current was 25%. In [15], the use of genetic algorithms is proposed to determine

the optimum quasi-square wave flux distribution in multiphase induction machines having a number of phases that is not a multiple of three, and the paper came to the conclusion that the contribution of field harmonics of order greater than five is negligible. In [16], an indirect vector control scheme is presented with an improved flux pattern using third harmonic injection. Compared with [12] and [13], the controller is designed such that the air-gap third harmonic is aligned with the fundamental harmonic in all loading conditions.

However, the study in [17], comparing different cases of high-torque-density induction machines from the point of view of the electromagnetic design, revealed that the high-order spatial harmonics produce higher losses in the stator back iron, which are usually neglected in the analysis of high-torque-density multiphase machines. To keep the same iron saturation, it was necessary to increase the stator back iron by about 20% in comparison with non-high-torque-density multiphase machines or three-phase machines, thus reducing their gain margin.

It is worth noting that the effect of the additional power loss in the stator back iron depends on the electromagnetic design, and therefore, it should be assessed from time to time.

Nevertheless, the capability to produce higher torque values is still interesting in overload conditions, where the output power and the output torque are limited mainly by the inverter constraints rather than by the motor losses.

The effect of the inverter constraints is shown in [18] and [19]. To summarize, the harmonic components added to the air-gap field are generated by magnetizing currents. Since the maximum inverter current is prefixed, the maximum torque is the result of a constrained optimization problem that determines the best combination of active and magnetizing currents. The result is that the injection of current harmonics can be useless for low torque values and has to be properly modulated for higher torque values.

A possible field of application for high-torque-density multiphase motors may be the electric traction, where there is an increasing demand of electric machines featuring high overload torque, magnet-free design, and field-weakening operation. Since the power is split among several phases, the current level is lower, and cheaper technologies, such as MOSFET switches (in parallel), can be adopted instead of insulated-gate bipolar transistor (IGBT) switches for the construction of the power inverter.

The development of robust control schemes for high-torque-density multiphase induction motor drives that are capable of exploiting the maximum torque at any speed has not been widely analyzed in the literature.

Concerning this problem, this paper improves the results reported in [20] by extending the analysis to the whole speed range (including field weakening). The analysis is focused on the effect of the constraints due to the machine and the inverter ratings on the optimization of the maximum torque.

The analysis leads to explicit expressions of the active and magnetizing currents that maximize the electromagnetic torque. The set-point values of these currents are updated online depending on the operating conditions. Furthermore, the control system needs only a small subset of the machine

parameters for the field-weakening operation, thus improving the robustness and reliability of the drive at high speed. The developed control technique is applied to a prototype of a seven-phase induction motor drive, and the performance is experimentally tested.

## II. MATHEMATICAL MODEL

The analysis developed here is valid for  $N$ -phase ( $N$  is an odd number greater than 3) squirrel-cage induction machines in which the arrangement of the stator windings, which is assumed star connected, is symmetrical. To adequately represent the behavior of such machines, it is necessary to consider the spatial components of the magnetic field in the air gap up to the  $(N - 2)$ th order. To obtain a compact formulation of the model, it is opportune to adopt the vector notation in multiple  $d-q$  planes (multiple space vectors) and to express the motor equations in reference frames in synchronism with the corresponding rotor flux vectors:

$$\bar{v}_{S\rho} = R_S \bar{i}_{S\rho} + j\omega_\rho \bar{\varphi}_{S\rho} + \frac{d\bar{\varphi}_{S\rho}}{dt}, \quad \rho = 1, 3, \dots, N - 2 \quad (1)$$

$$0 = R_{R\rho} \bar{i}_{R\rho} + j(\omega_\rho - \rho\omega_m)\bar{\varphi}_{R\rho} + \frac{d\bar{\varphi}_{R\rho}}{dt}, \quad \rho = 1, 3, \dots, N - 2 \quad (2)$$

$$\bar{\varphi}_{S\rho} = L_{S\rho} \bar{i}_{S\rho} + M_\rho \bar{i}_{R\rho}, \quad \rho = 1, 3, \dots, N - 2 \quad (3)$$

$$\bar{\varphi}_{R\rho} = M_\rho \bar{i}_{S\rho} + L_{R\rho} \bar{i}_{R\rho}, \quad \rho = 1, 3, \dots, N - 2 \quad (4)$$

$$T = \frac{N}{2} p \sum_{\rho=1,3,\dots,N-2} \rho M_\rho \bar{i}_{S\rho} \cdot j \bar{i}_{R\rho} \quad (5)$$

where  $T$  is the electromagnetic torque;  $p$  is the pole pairs;  $\omega_\rho$  is the angular speed of the  $\rho$ th rotor flux vector;  $\omega_m$  is the rotor angular speed in electric radians per second;  $\bar{i}_{S\rho}$  and  $\bar{i}_{R\rho}$  ( $\rho = 1, 3, \dots, N - 2$ ) are the multiple space vectors of the stator and rotor currents, respectively;  $\bar{\varphi}_{S\rho}$  and  $\bar{\varphi}_{R\rho}$  ( $\rho = 1, 3, \dots, N - 2$ ) are the multiple space vectors of the stator and rotor fluxes, respectively; and  $L_{S\rho}$ ,  $L_{R\rho}$ , and  $M_\rho$  ( $\rho = 1, 3, \dots, N - 2$ ) are parameters that can be interpreted as self-inductance and mutual inductance, respectively.

In the mathematical model described by (1)–(5), iron losses are ignored, the permeability of the iron core is infinite, and the saturation and the slot effect are not considered.

As can be seen from (1)–(5), an  $N$ -phase induction machine can be decomposed into  $(N - 1)/2$  independent three-phase induction machines (denoted by indexes  $1, 3, \dots, N - 2$ ) sharing the same shaft. The current space vectors  $\bar{i}_{S\rho}$  and  $\bar{i}_{R\rho}$  are responsible for the generation of the  $\rho$ th spatial component of the magnetic field in the air gap.

## III. CONSTRAINT ON THE AIR-GAP FLUX DENSITY

High-order spatial harmonics of the air-gap magnetic field can be effectively controlled in multiphase machines with concentrated windings (i.e., with one slot per pole per phase). If these harmonics are synchronized with the fundamental component, it is possible to increase the amplitude of the

fundamental component without changing the peak value  $H_M$  of the resulting total field wave, which is usually chosen so that the iron core does not incur excessive magnetic saturation.

### A. Amplitude of the Air-Gap Flux Density

To simplify the analysis, it is assumed that the motor is only excited by the fundamental and third harmonic components of the voltages.

The resultant magnetic field can be written as follows:

$$H(\theta) = H_1 \cos(\theta) - H_3 \cos(3\theta) \quad (6)$$

where  $\theta$  is an angular coordinate; and  $H_1$  and  $H_3$  are the amplitudes of the fundamental and third harmonic components of the magnetic field, respectively. The angle  $\theta$  is expressed in electrical radians and varies within the range  $[-\pi/2, \pi/2]$  in a pole pitch.

For a fair comparison and to maintain the same level of iron saturation, the maximum value of (6) should be limited to  $H_M$ , i.e.,

$$\max_{-\frac{\pi}{2} \leq \theta \leq \frac{\pi}{2}} \{H_1 \cos(\theta) - H_3 \cos(3\theta)\} = H_M. \quad (7)$$

Ignoring leakage fluxes, (7) can be written in terms of the flux-producing currents  $I_{S1d}$  and  $I_{S3d}$  instead of  $H_1$  and  $H_3$ . The currents  $I_{S1d}$  and  $I_{S3d}$  are the  $d$ -components of the stator current vectors in the  $d_1-q_1$  and  $d_3-q_3$  frames, which are aligned with the rotor flux vectors corresponding to the first and third spatial harmonics of the magnetic field.

Consequently, the following equation can be obtained:

$$\max_{\theta \in [-\frac{\pi}{2}, \frac{\pi}{2}]} \left\{ I_{S1d} \cos(\theta) - \frac{I_{S3d}}{3} \cos(3\theta) \right\} = I_{Sd, \text{rated}} \quad (8)$$

where  $I_{Sd, \text{rated}}$  is the rated magnetizing current of the machine, i.e., the magnetizing current that produces the rated sinusoidal spatial distribution of the air-gap magnetic field.

Defining the following current ratio:

$$\eta = \frac{I_{S3d}}{I_{S1d}} \quad (9)$$

(8) can be written as

$$C(\eta) I_{S1d} = I_{Sd, \text{rated}} \quad (10)$$

where  $C(\eta)$  is as follows:

$$C(\eta) = \max_{\theta \in [-\frac{\pi}{2}, \frac{\pi}{2}]} \left\{ \cos(\theta) - \frac{\eta}{3} \cos(3\theta) \right\}. \quad (11)$$

The analytical expression of  $C(\eta)$  is given by (12), and its variation with respect to  $\eta$  is depicted in Fig. 1. Thus,

$$C(\eta) = \begin{cases} 1 - \frac{1}{3}\eta, & \text{if } \eta \leq \frac{1}{3} \\ \frac{1}{3}(\eta + 1) \sqrt{1 + \frac{1}{\eta}}, & \text{otherwise.} \end{cases} \quad (12)$$

The function  $C(\eta)$  expresses the reduction in the peak value of the field wave due to the third spatial harmonic component.

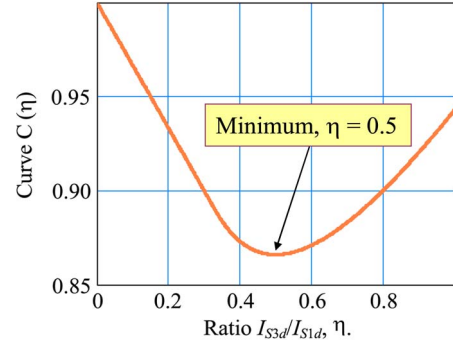


Fig. 1. Behavior of the curve  $C(\eta)$ .

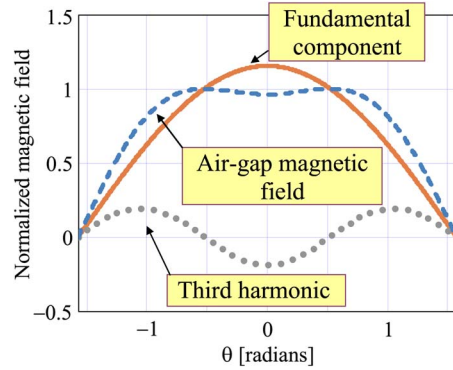


Fig. 2. Waveform of the air-gap magnetic field: fundamental component and third spatial harmonic.

Both  $C(\eta)$  and its derivative are continuous functions; thus, it is straightforward to verify that the absolute minimum of  $C(\eta)$  is at

$$\eta_m = \frac{1}{2}. \quad (13)$$

Therefore, the components of the stator current in the  $d_1$ - and  $d_3$ -axes can be written as

$$I_{S1d, \text{max}} = \frac{2}{\sqrt{3}} I_{Sd, \text{rated}} \quad (14)$$

$$I_{S3d, \text{max}} = \frac{1}{\sqrt{3}} I_{Sd, \text{rated}}. \quad (15)$$

The maximum value of  $H_1$  is  $2/\sqrt{3}H_M$ , and  $H_3$  is  $1/6$  of  $H_1$ . The fundamental and third harmonic components and the resultant waveforms of the air-gap field are illustrated in Fig. 2.

### B. Synchronization of the Field Wave

Since the  $d_1$ - and  $d_3$ -axes are aligned with rotor flux vectors  $\bar{\varphi}_{R1}$  and  $\bar{\varphi}_{R3}$ , respectively, there will be no  $q$ -axes component for rotor flux. Combining (2) and (4) for  $\rho = 1$  and considering only the  $q$ -component, the slip frequency  $\omega_1 - \omega_m$  can be obtained as a function of current  $i_{S1q}$  as follows:

$$\tau_{R1}(\omega_1 - \omega_m)\varphi_{R1} = M_1 i_{S1q} \quad (16)$$

where  $\tau_{R1}$  is the ratio of  $L_{R1}$  to  $R_{R1}$ .

Similarly, by combining (2) and (4) for third-order harmonic ( $\rho = 3$ ), one obtains

$$\tau_{R3}(\omega_3 - 3\omega_m)\varphi_{R3} = M_3 i_{S3q} \quad (17)$$

where  $\tau_{R3}$  is the ratio of  $L_{R3}$  to  $R_{R3}$ .

If the third spatial harmonic of the magnetic field is synchronized with the fundamental component, its electric angular speed is triple that of the fundamental wave, i.e.,

$$\omega_3 = 3\omega_1. \quad (18)$$

Substituting (18) into (17) and considering (16), it results that that the synchronism is possible only if the following condition holds true:

$$\frac{3\tau_{R3}\varphi_{R3}}{\tau_{R1}\varphi_{R1}} = \frac{M_3 i_{S3q}}{M_1 i_{S1q}}. \quad (19)$$

In steady-state condition, the fundamental and third-order harmonics of the rotor flux are proportional to the  $d_1$  and  $d_3$  components of the stator current, i.e.,

$$\varphi_{R1} = M_1 i_{S1d} \quad (20)$$

$$\varphi_{R3} = M_3 i_{S3d}. \quad (21)$$

Substituting (20) and (21) into (19), one comes to the following result:

$$I_{S3q} = \frac{3\tau_{R3}}{\tau_{R1}} \eta I_{S1q}. \quad (22)$$

The preceding equation is used in Section IV to obtain the correct value of the current  $i_{S3q}$  so that the magnetic field wave generated by the stator current vector  $\vec{i}_{S3}$  is in synchronism with the one generated by current vectors  $\vec{i}_{S1}$  and  $\vec{i}_{R1}$ .

## IV. MAXIMIZATION OF THE MOTOR TORQUE

### A. Problem Statement

If the air-gap magnetic field only consists of the fundamental and third spatial harmonics, the expression of the steady-state torque of an  $N$ -phase motor can be written as follows:

$$T = \frac{pN}{2} \left( \frac{M_1^2}{L_{R1}} I_{S1d} I_{S1q} + 3 \frac{M_3^2}{L_{R3}} I_{S3d} I_{S3q} \right). \quad (23)$$

Equation (23) shows that the magnetic torque is a function of the four steady-state current components  $I_{S1d}$ ,  $I_{S1q}$ ,  $I_{S3d}$ , and  $I_{S3q}$  of the stator current vectors.

Let us assume that the RMS value of phase current is  $I_S/\sqrt{2}$ . The relationship between the RMS value of the stator current and the  $d$ - $q$  axes components of current is as follows:

$$I_S^2 = I_{S1d}^2 + I_{S1q}^2 + I_{S3d}^2 + I_{S3q}^2. \quad (24)$$

The inverter current rating and the machine thermal rating set a limit value, i.e.,  $I_M$ , for the phase current  $I_S$ . For a given  $I_S$ , the maximum achievable torque corresponds to a precise combination of the current components and results from a constrained optimization of (23) subjected to the constraints (9),

(10), (22), and (24). The formal statement of the optimization problem is reported in the Appendix.

Substituting (9) and (22) into (23) and (24) and considering that  $M_3$  is 1/9 of  $M_1$  in induction motors without rotor skew, the torque can be expressed as

$$T = \frac{pN}{2} \frac{M_1^2}{L_{R1}} I_{S1d} I_{S1q} (1 + \alpha \eta^2) \quad (25)$$

where

$$\alpha = \frac{1}{9} \frac{L_{R1} \tau_{R3}}{L_{R3} \tau_{R1}} = \frac{R_{R1}}{9 R_{R3}} \quad (26)$$

whereas the stator current can be written as

$$I_{S1d}^2 (1 + \eta^2) + I_{S1q}^2 [1 + \beta \eta^2] = I_S^2 \quad (27)$$

where

$$\beta = 9 \left( \frac{\tau_{R3}}{\tau_{R1}} \right)^2. \quad (28)$$

As a result, (25) shows that the motor torque is proportional to the current  $I_{S1q}$  and seems to increase as  $\eta$  increases. However, (27) reveals that, if  $\eta$  is not zero, there is a reduction in the maximum current  $I_{S1q}$  available for generating the magnetic torque. In other words, since the constraints are nonlinear, the optimization is not trivial.

### B. Approximate Solution

An approximate solution of constrained maximization of (25) was found in [18] and [19], where it was shown that  $\eta_{\text{opt}}$  can be approximated as a function of the ratio  $I_{Sd,\text{rated}}/I_S$ , i.e.,

$$\eta_{\text{opt}} = \begin{cases} \eta_0 + \frac{1}{\delta^2} \left( \frac{1}{3} - \eta_0 \right) \left( \frac{I_{Sd,\text{rated}}}{I_S} \right)^2, & \text{if } \frac{I_{Sd,\text{rated}}}{I_S} \leq \delta \\ \frac{\frac{\sqrt{2}}{2} - \frac{I_{Sd,\text{rated}}}{I_S}}{3 \left( \frac{\sqrt{2}}{2} - \delta \right)}, & \text{if } \delta < \frac{I_{Sd,\text{rated}}}{I_S} < \frac{\sqrt{2}}{2} \\ 0, & \text{if } \frac{I_{Sd,\text{rated}}}{I_S} \geq \frac{\sqrt{2}}{2} \end{cases} \quad (29)$$

where  $\eta_0$  and  $\delta$  are defined as

$$\delta = 12 \frac{\sqrt{(3\alpha\beta + 47\alpha - 13\beta + 63)(\alpha\beta + 17\alpha - 7\beta + 9)}}{27\alpha\beta + 423\alpha - 117\beta + 567} \quad (30)$$

$$\eta_0 = -\frac{1}{4} \frac{\frac{\alpha^2\beta + \alpha\beta^2}{16} - \frac{11(\alpha^2 + \beta^2)}{8} + \frac{7\alpha\beta}{2} + \alpha + \beta + 2}{\frac{7\alpha^2\beta}{64} - \frac{\alpha\beta^2}{32} + \frac{17\alpha^2}{16} + \frac{\beta^2}{2} - \frac{11\alpha\beta}{8} + \alpha - \frac{5\beta}{4} - 1}. \quad (31)$$

It is worth noting that, since  $\alpha$  and  $\beta$  are usually small quantities, the values of  $\eta_0$  and  $\delta$  are nearly 0.5.

Although (29) is a function of  $I_{Sd,\text{rated}}/I_S$ , the behavior of  $\eta_{\text{opt}}$  can be better understood when it is plotted as a function of  $I_S/I_{Sd,\text{rated}}$ , as shown in Fig. 3, which compares the exact solution with the approximated analytical solution (29).

The parameters adopted to draw the curve in Fig. 3 are those in Table I and are the same as those of the electric motor drive used during the experimental tests described in

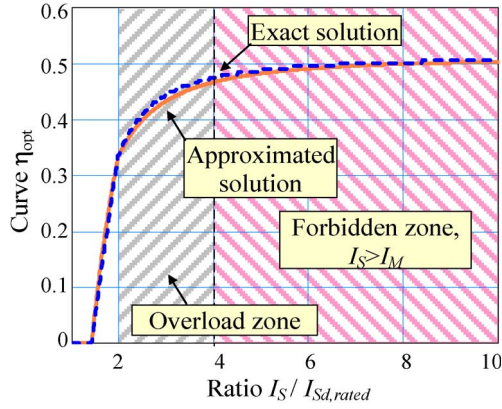


Fig. 3. Trend of the curve  $\eta_{opt}$  as a function of the ratio  $I_S / I_{Sd,rated}$  (the pink zone is forbidden, since the stator current should be lower than  $I_M$ ).

TABLE I  
MOTOR PARAMETERS

$N$	$= 7$	$L_{S1} = 175$ mH	$R_S = 1.3$ $\Omega$
$p$	$= 2$	$L_{S3} = 24$ mH	$R_{R1} = 1.1$ $\Omega$
$T_{rated}$	$= 28$ Nm	$M_1 = 170$ mH	$R_{R3} = 0.9$ $\Omega$
$I_M$	$= 10$ A	$M_3 = 19$ mH	$\alpha = 0.139$
$I_{s,rated}$	$= 5$ A <sub>pk</sub>	$L_{R1} = 175$ mH	$\beta = 0.261$
$I_{Sd,rated}$	$= 2.5$ A <sub>pk</sub>	$L_{R3} = 24$ mH	$E_{dc} = 160$ V

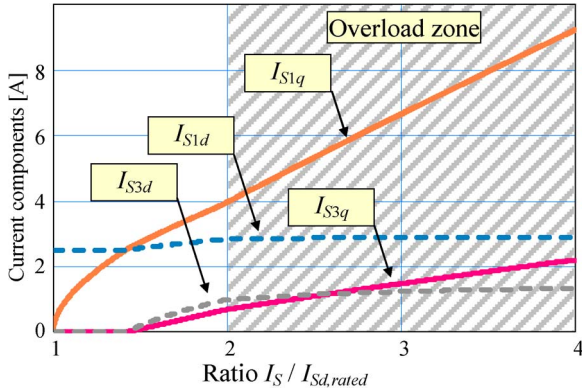


Fig. 4. Trends of the components of the stator current vectors as functions of  $I_{Sd,rated} / I_S$ .

Section VII. Basically, when  $I_S$  is lower than  $\sqrt{2} I_{Sd,rated}$ , the injection of the third harmonic current is useless or even detrimental, because it reduces the current  $I_{S1q}$  available for torque generation. Conversely, when  $I_S$  is much greater than  $I_{Sd,rated}$ ,  $\eta_{opt}$  reaches a value that is around 0.5 and depends weakly on the machine parameters. However, the maximum value of  $\eta_{opt}$  can be unreachable. In nominal operating conditions, the ratio  $I_S / I_{Sd,rated}$  of the machine used as example in this paper is 2, and the parameter  $\eta_{opt}$  is 0.3. If the machine operates in overload condition (dashed zone in Fig. 3), the ratio  $I_S / I_{Sd,rated}$  can increase up to 4, and the parameter  $\eta_{opt}$  becomes 0.47. Higher values of current are not possible, because they are greater than the maximum inverter current  $I_M$ .

Finally, the values of the components of the stator current vectors corresponding to the maximum torque are shown in Fig. 4.

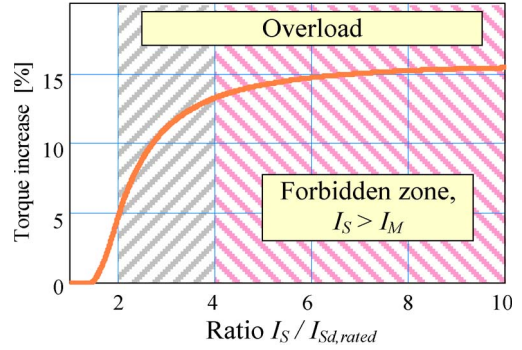


Fig. 5. Percentage of increase in the magnetic torque due to the third harmonic injection as a function of  $I_{S1q}$ .

### C. Torque Improvement

Once  $\eta_{opt}$  is known, it is possible to calculate  $I_{S1d}$  and  $I_{S1q}$  by solving (10) and (27), i.e.,

$$I_{S1d} = \frac{I_{Sd,rated}}{C(\eta_{opt})} \tag{32}$$

$$I_{S1q} = \pm \sqrt{\frac{I_S^2 - \left(\frac{I_{Sd,rated}}{C(\eta_{opt})}\right)^2 (1 + \eta_{opt}^2)}{1 + 9 \left(\frac{\tau_{R3}}{\tau_{R1}}\right)^2 \eta_{opt}^2}} \tag{33}$$

The electromagnetic torque can be found by substituting (32) and (33) into (25). Since  $\eta_{opt}$  is a function of  $I_S$ , the torque turns out to be a function of  $I_S$  as well.

Fig. 5 shows the increase in the optimized torque compared with the absence of the third harmonic component of the air-gap field. If  $I_S$  is lower than  $\sqrt{2} I_{Sd,rated}$ , no improvement is possible. On the contrary, if  $I_S$  is sufficiently greater than  $\sqrt{2} I_{Sd,rated}$ , the increase in the torque is around 5% at the rated current. In overload conditions, it can be up to 13% and is limited by the maximum admissible current  $I_M$ .

## V. OPERATING SPEED RANGES

At high speed, the motor operation is limited not only by the inverter current rating and the machine thermal rating but also by the available dc-link voltage.

Therefore, to analyze the operating speed ranges, it is required to find the maximum voltage vectors that can be applied to the machine.

### A. Voltage Constraint

DC-link voltage utilization depends on the modulation technique being used. Hereafter, it is assumed that the applied modulation technique is capable of fully exploiting the dc-link voltage and generating all possible combinations of voltage vectors in the  $d-q$  planes. For example, modulation strategies with these features are the carrier-based pulsewidth modulation (PWM) with a suitable choice of the zero-sequence voltage or the space vector modulation [20]–[25].

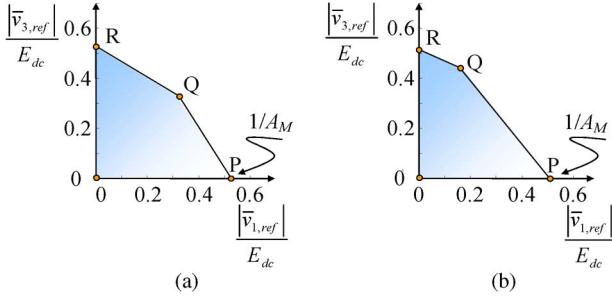


Fig. 6. Validity domains of  $v_{1,\text{ref}}$  and  $v_{3,\text{ref}}$ , normalized by the dc-link voltage  $E_{dc}$ . (a) Five-phase inverters. (b) Seven-phase inverters.

Due to high number of degrees of freedom, finding the output voltage limit of multiphase inverters requires more computational effort. An approximate explicit solution for the voltage boundary of a seven-phase inverter has been found in [26], and it has been extended for  $N$ -phase inverters in [27]. If  $N$  is a prime number, the constraints acting on the magnitude of the voltage vectors can be written as a set of linear inequalities, linking the magnitudes of the multiple voltage space vectors, independent of their phase angles, i.e.,

$$\sum_{\rho=1,3,\dots,N-2} A_{\rho,h} |\bar{v}_{\rho,\text{ref}}| \leq E_{dc}, \quad h = 1, 2, \dots, \frac{N-1}{2} \quad (34)$$

where

$$A_{\rho,h} = 2 \left| \sin \frac{\pi \rho}{N} h \right|. \quad (35)$$

As a consequence, the dc-link voltage that is necessary to synthesize the voltage vectors  $\bar{v}_{1,\text{ref}}, \bar{v}_{3,\text{ref}}, \dots, \bar{v}_{N-2,\text{ref}}$  is equal to

$$E_{dc,\text{req}} = \max_{h=1,2,\dots,\frac{N-1}{2}} \left\{ \sum_{\rho=1,3,\dots,N-2} A_{\rho,h} |\bar{v}_{\rho,\text{ref}}| \right\}. \quad (36)$$

Under the assumption that the magnitude of the voltage vectors with  $\rho > 3$  is zero, (36) can be simplified and becomes

$$E_{dc,\text{req}} = \max_{h=1,2,\dots,\frac{N-1}{2}} \{A_{1,h} v_{1,\text{ref}} + A_{3,h} v_{3,\text{ref}}\} \quad (37)$$

whereas, if only  $\bar{v}_{1,\text{ref}}$  is nonzero, (36) becomes

$$E_{dc,\text{req}} = A_M v_{1,\text{ref}} \quad (38)$$

where

$$A_M = \max_{h=1,2,\dots,\frac{N-1}{2}} \{A_{1,h}\} = 2 \sin \left( \frac{\pi}{2} \frac{N-1}{N} \right). \quad (39)$$

Fig. 6, which can be generated using (37), shows the admissible magnitudes of the voltage vectors  $\bar{v}_{1,\text{ref}}$  and  $\bar{v}_{3,\text{ref}}$  corresponding to a given level of the dc-link voltage  $E_{dc,\text{req}}$  for five- and seven-phase inverters. As can be seen, the admissible voltage regions are slightly different depending on the number of phases. This result may slightly change the operating speed range of the machine. This aspect is analyzed in the next subsection.

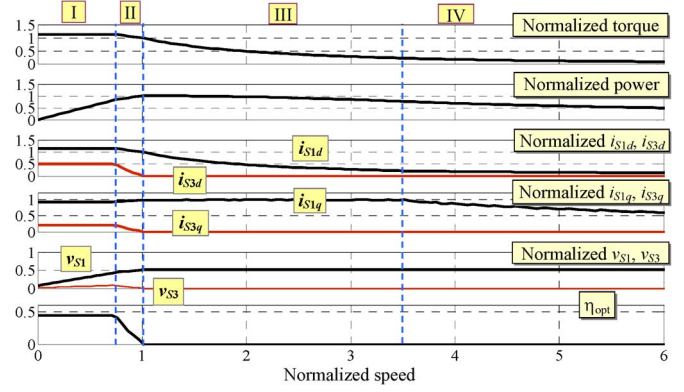


Fig. 7. Maximum torque capability of the seven-phase motor with parameters reported in Table I. Torque and power are normalized by the respective nominal values. The currents on the  $d$ -axes are normalized by  $I_{Sd,\text{rated}}$ . The currents on the  $q$ -axes are normalized by  $I_M$ . The voltages are normalized by  $E_{dc}$ . The speed is normalized by the base speed.

## B. Operation at High Speed

Equations (1)–(12) can be used to model a multiphase machine and calculate the best set of values for  $d$ -axes currents  $i_{S1d}$  and  $i_{S3d}$  that maximizes the torque capability of the motor at any speed without exceeding the current limit  $I_M$ , the voltage limit, and the peak value of the air-gap flux density.

The result of this optimization procedure, under the assumption that the motor parameters are those in Table I, is shown in Fig. 7.

Although the example in Fig. 7 refers to a seven-phase motor, the behavior seems quite general and can be valid for all multiphase induction machines. In essence, four different speed ranges can be identified.

At low speed (region I), the third-order spatial harmonic of the air-gap field can be used to increase the maximum motor torque without changing the current absorption, which is limited by the maximum current  $I_M$ .

Region II begins as soon as the dc-link voltage is insufficient. As the speed increases, the control system progressively reduces  $i_{S3d}$ , and the torque enhancement becomes impossible, because the back electromotive force (EMF) due to the third-order harmonic of the magnetic field would require an excessive portion of the dc-link voltage to the detriment of the fundamental harmonic, which is actually responsible for the most part of the electromagnetic torque. Furthermore, reducing  $i_{S3}$  allows a small increase in  $i_{S1q}$  and consequently helps to restrain the torque reduction.

In region III, i.e., at speeds higher than the base speed, the maximum power generated by the machine is nearly constant and slightly greater than the power at base speed. The RMS value of the phase current is constant, and the voltage limit is completely exploited by  $v_{S1}$  alone.

Finally, at very high speed (region IV), the dc-link voltage is not sufficient to inject the maximum current into the motor phases. The power delivered to the load decreases, and the motor behavior, like in region III, is very similar to that of a traditional three-phase motor. The condition for the maximum torque is that the stator flux vector and the rotor flux vector form an angle of  $45^\circ$ , i.e., the  $d$ -component of the stator flux vector,

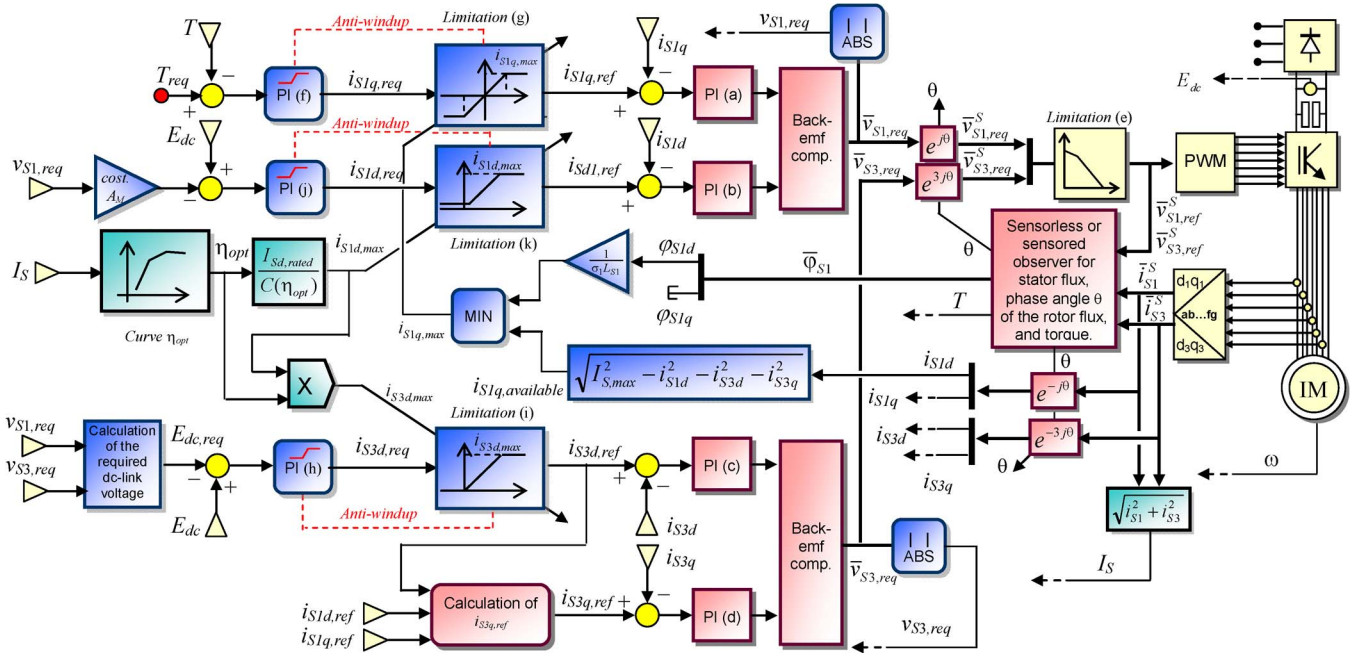


Fig. 8. Block diagram of the control scheme.

expressed in the synchronous reference frame, is equal to the  $q$ -component [28].

### C. No Harmonic Injection in Field-Weakening Speed Range

Above the base speed, the injection of the third spatial harmonic is not useful. This result is generally valid and can be proven by the following reasoning. For the sake of simplicity, let us focus only on the operating conditions around the base speed, when the inverter capability is completely exploited and the voltage limit (34) becomes an equality. In this case, (34) can be rewritten in the following form:

$$A_1 v_{1,\text{ref}} + A_3 v_{3,\text{ref}} = E_{dc} \quad (40)$$

where  $A_1$  and  $A_3$  are positive coefficients depending on the number of phases. For example, (40) may correspond to segment PQ in Fig. 6(a) and (b).

If the voltage drops on the stator resistances are negligible and the steady-state operation is assumed, the derivative of the torque can be calculated with respect to  $\eta$  under the constraints (10), (22), and (26), in the nominal operating conditions, i.e.,

$$I_{S1d} = I_{Sd,\text{rated}} \quad (41)$$

$$I_{S1q} = \sqrt{I_M^2 - I_{Sd,\text{rated}}^2} \quad (42)$$

$$I_{S3d} = I_{S3q} = 0 \quad (43)$$

$$\eta = 0. \quad (44)$$

The result is as follows:

$$\frac{dT}{d\eta} = Np \frac{M_1^2}{L_{R1}} \frac{d}{d\eta} (I_{S1q}^2 - I_{S1d}^2) \quad (45)$$

where

$$d = 3A_3 L_{S3} \sqrt{I_{S1d}^2 + 9\sigma_3^2 \left(\frac{\tau_{R3}}{\tau_{R1}}\right)^2 I_{S1q}^2} \quad (46)$$

$$\Delta = -\frac{2I_{S1d}I_{S1q}A_1L_{S1}(1 - \sigma_1^2)}{\sqrt{I_{S1d}^2 + \sigma_1^2 I_{S1q}^2}}. \quad (47)$$

Typically,  $I_{S1q}$  is greater than  $I_{S1d}$ , the parameter  $d$  is positive, and the parameter  $\Delta$  is negative. As a consequence, the derivative (45) is lower than zero, meaning that any increase in the amplitude of the third spatial harmonic has the effect of reducing the electromagnetic torque as long as (40) holds. This result is qualitatively also valid at higher speeds, since the machine speed is not among the variables appearing in (45)–(47).

## VI. CONTROL SCHEME

A control scheme based on the results obtained in Section IV has been developed, and its block diagram is shown in Fig. 8, which can be ideally divided into three sections with different aims. The first section concerns the current control loop, the second one is the tracking of torque reference, whereas the third one ensures the robust field-weakening operation. In Fig. 8, the controlled variables are expressed in two reference frames  $d_1-q_1$  and  $d_3-q_3$ , which are synchronized and aligned with the corresponding rotor flux vectors. For the proper operation of the control scheme, it is assumed that motor fluxes, torque, and speed can be estimated.

### A. Current Loops

The reference signals  $i_{S1d,\text{ref}}$  and  $i_{S1q,\text{ref}}$  are tracked by means of proportional–integral (PI) regulators (a) and (b),

whereas the reference signals  $i_{S3d,ref}$  and  $i_{S3q,ref}$  are tracked by means of PI regulators (c) and (d). The estimated values of the back EMFs are added to the output signals of the previous regulators to improve the tracking dynamics. If the available voltage of the dc link is insufficient to synthesize the requested voltage vectors, limitation block (e) proportionally reduces the magnitude of the request voltage vectors, so that the rescaled reference voltages can fit in the linear modulation area in Fig. 6.

It is worth noting that additional PI regulators, which are not shown in Fig. 8 for the sake of simplicity, must keep the current vectors  $\bar{i}_{S\rho}$  for  $\rho > 3$  equal to zero to avoid that small voltage disturbances, such as those caused by the inverter dead times or by a phase unbalance, may induce undesired circulating currents.

### B. High Torque Density

Once the stator currents have been measured and the ratio  $I_S/I_{Sd,rated}$  is known, (27) provides the value of  $\eta_{opt}$ , upon which the calculation of the optimal value of the current  $i_{S3d}$  depends. This value is regarded as an upper bound for  $i_{S3d}$ , and it is called  $i_{S3d,max}$  in Fig. 8, because  $i_{S3d}$  can be lower than  $i_{S3d,max}$  when the dc-link voltage is insufficient to inject the requested current. Finally, if the stator current is smaller than  $\sqrt{2}I_{Sd,rated}$ ,  $\eta_{opt}$ , and  $i_{S3d,max}$  are both zero, and the high-torque-density operation is disabled.

### C. Torque Loop

The PI regulator (f) receives the tracking error between the torque set point and the estimated torque as input signal, and it adjusts the request of the torque-producing current  $i_{S1q,req}$ , which is proportional to the electromagnetic torque. Afterward, (22) allows one to calculate as a function of  $i_{S1d,ref}$  and  $i_{S1q,ref}$  the reference value  $i_{S3q,ref}$  that is necessary to synchronize the fundamental component of the magnetic field with the third-order spatial harmonic.

In regions I–III, the maximum deliverable torque is limited by the maximum current  $I_{s,max}$ , whereas in region IV, the maximum torque takes places when the  $d$ -component of the stator flux vector is equal to the  $q$ -component of the stator flux vector. In steady-state condition, this latter equality can be written as follows [28]:

$$i_{S1q} = \frac{\varphi_{S1d}}{\sigma_1 L_{S1}}. \quad (48)$$

The limitation block (g) assures that these constraints are satisfied in any speed region. In fact, the absolute value of current  $i_{S1q}$  is bounded by  $i_{S1q,max}$ , which makes the stator current equal to  $I_{s,max}$  or makes  $\varphi_{S1q}$  equal to  $\varphi_{S1d}$ , depending on which one is the most restrictive constraint in the actual operating condition.

### D. Flux Loop

The PI regulators (j) and (h) generate the  $d$ -axis components of stator currents  $i_{S1d,req}$  and  $i_{S3d,req}$ , which, in turn, adjust

the rotor flux magnitudes  $\varphi_{R1}$  and  $\varphi_{R3}$ . When the motor speed is too high, the available dc-link voltage  $E_{dc}$  is not sufficient to entirely satisfy the voltage request, which is represented by  $E_{dc,req}$ .

If  $E_{dc}$  is persistently lower than  $E_{dc,req}$ , then the motor is operating in region II, region III, or region IV; and the third spatial harmonic of the magnetic field has to decrease. This task is implemented by PI regulator (h), which integrates the difference of  $E_{dc}$  and  $E_{dc,req}$ . If this difference is negative,  $i_{S3d}$  is set to zero. Otherwise, it increases up to the threshold value  $i_{S3d,max}$  shown in the  $d_3$ -axis current limiter block (i) and calculated based on  $\eta_{opt}$ .

It is worth noting that the reduction in  $i_{S3d}$  leads to a reduction in the requested voltage. As a consequence, in region II, as long as  $v_{S1,req}$  is lower than  $E_{dc}/A_M$ , it is possible to keep  $\varphi_{R1}$  unaltered.

Conversely, in regions III and IV, the voltage request  $v_{S1,req}$  is greater than  $E_{dc}/A_M$ , and it can never be satisfied, even if the third harmonic of the magnetic field is set to zero. In this case, PI regulator (j), which integrates a quantity proportional to the difference  $E_{dc} - A_M v_{S1,req}$ , decreases  $\varphi_{R1}$  by acting on the current  $i_{S1d}$ . The  $d_1$ -axis current limiter (k) limits this current to an upper bound  $i_{S1d,max}$ , given by (14), and a lower bound  $i_{S1d,min}$ , ensuring the stable operation of the motor at high speed.

The only motor parameter that is necessary for the field-weakening operation is the leakage inductance  $\sigma_1 L_{S1}$ , which is already used in the state observer in most cases. In addition, the knowledge of the base speed is not necessary, as well as complex calculations of the flux level or lookup tables.

## VII. EXPERIMENTAL RESULTS

An experimental testbed consisting of a seven-phase IGBT-based inverter and a 2-kW seven-phase squirrel-cage induction motor has been built to verify the theoretical findings. The motor parameters are the same as those listed in Table I. In [29]–[32], various methodologies have been proposed for the determination of these parameters. The simplest way is to perform no-load and blocked-rotor tests by feeding the motor with one voltage vector at a time. The modulation technique used to control the seven-phase inverter is the PWM strategy described in [26].

Figs. 9 and 10 show the behavior of the motor during two step changes of the torque reference, from 0 to 5 N · m and from 5 N · m to the maximum torque, at low speed. The maximum torque theoretically depends on the machine parameters, the operating conditions, and the maximum admissible current  $I_M$ . In practice, during the experimental tests, the torque request has been set to a value that is certainly greater than the maximum one, so that the control system is forced to produce the highest possible torque, corresponding to about 32 N · m.

Both figures show the waveforms of the estimated torque and the stator current, but Fig. 9 shows also the waveforms of  $i_{S1d,ref}$  and  $i_{S3d,ref}$ , whereas Fig. 10 shows the waveforms of  $i_{S1q,ref}$  and  $i_{S3q,ref}$ .

The current that is necessary to produce 5 N · m is about 3 A. This value is below the threshold  $\sqrt{2} I_{Sd,rated}$ , equal to 3.5 A,

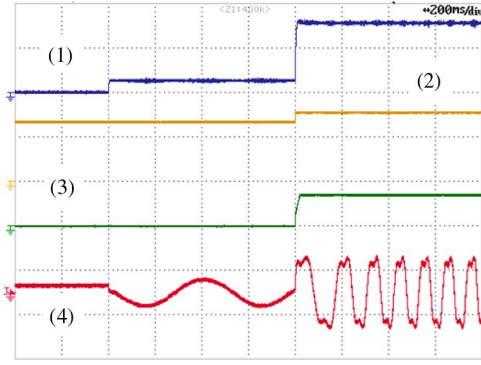


Fig. 9. Step changes of the torque from 0 to 5 N · m and from 5 N · m to the maximum value, at low speed. (1): motor torque (20 N · m/div); (2):  $i_{S1d}$  (2 A/div); (3):  $i_{S3d}$  (2 A/div); (4): stator current (10 A/div).

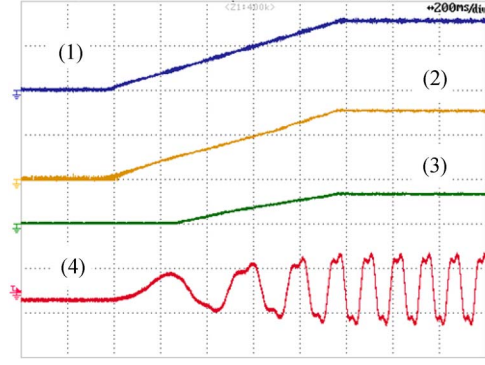


Fig. 12. Step changes of the torque from 0 N · m to the maximum value. (1): motor torque (20 N · m/div); (2):  $i_{S1q}$  (6 A/div); (3):  $i_{S3q}$  (3 A/div); (4): stator current (10 A/div).

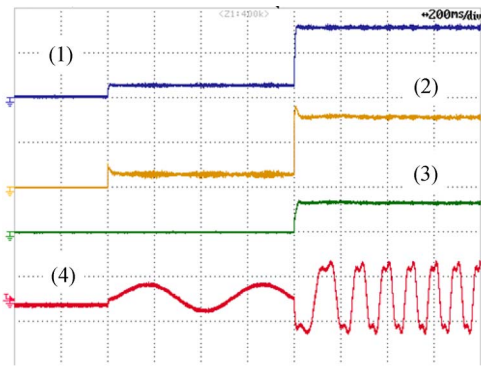


Fig. 10. Step changes of the torque from 0 to 5 N · m and from 5 N · m to the maximum value, at low speed. (1): motor torque (20 N · m/div); (2):  $i_{S1q}$  (6 A/div); (3):  $i_{S3q}$  (3 A/div); (4): stator current (10 A/div).

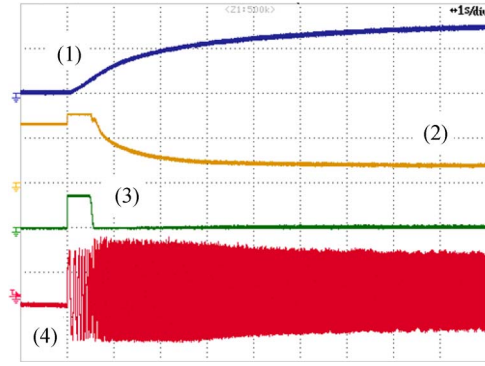


Fig. 13. Step change of the torque from 0 to the maximum value. (1): motor speed (2000 r/min/div); (2):  $i_{S1d}$  (2 A/div); (3):  $i_{S3d}$  (2 A/div); (4): stator current (10 A/div).

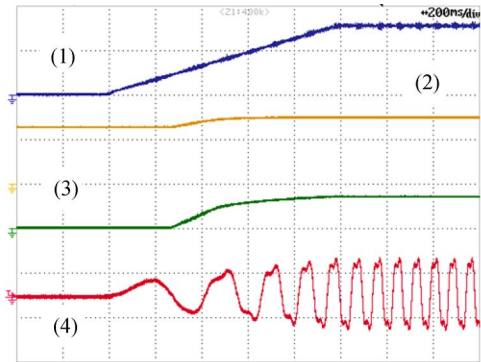


Fig. 11. Ramp command of the torque from 0 N · m to the maximum value. (1): motor torque (20 N · m/div); (2):  $i_{S1d}$  (2 A/div); (3):  $i_{S3d}$  (2 A/div); (4): stator current (10 A/div).

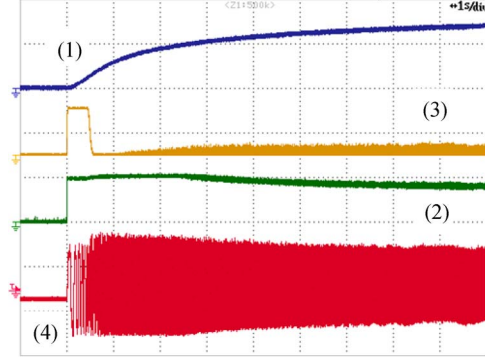


Fig. 14. Step change of the torque from 0 to the maximum value. (1): motor speed (2000 r/min/div); (2):  $i_{S1q}$  (2 A/div); (3):  $i_{S3q}$  (10 A/div); (4): stator current (10 A/div).

beyond which the use of third spatial harmonic of the magnetic field becomes useful. Consequently, at the beginning of the test, the stator currents are sinusoidal, and  $i_{S1d}$  is equal to  $I_{Sd, rated}$ . After the second torque step, the motor operates in overload conditions, since the stator current is twice the rated thermal current of the motor. The value of  $\eta_{opt}$  becomes about 0.46,  $i_{S3d}$  and  $i_{S3q}$  increase, and the waveform of the stator current is clearly distorted owing to the presence of the third harmonic.

Figs. 11 and 12 show the behavior of the drive during a ramp variation of the torque command from 0 N · m to the maximum torque. As soon as  $I_{S1d, ref}$  increases,  $I_{S3d, ref}$  increases to

reduce the peak value of the magnetic field, in such a way that the iron saturation remains constant. Figs. 11 and 12 clearly show the transition between the normal operation and the high-torque-density operation.

Figs. 13 and 14 show the waveforms of  $i_{S1d}$  and  $i_{S3d}$ ,  $i_{S1q}$  and  $i_{S3q}$ , respectively, during a step change of the torque command from 0 to the maximum torque. Traces (1) and (4) in Figs. 13 and 14 show the waveforms of the rotor speed and line current, respectively. In addition, Fig. 13 shows the waveforms of the currents  $i_{S1d}$  and  $i_{S1q}$ , whereas Fig. 14 shows the waveforms of the currents  $i_{S3d}$  and  $i_{S3q}$ . Initially, the

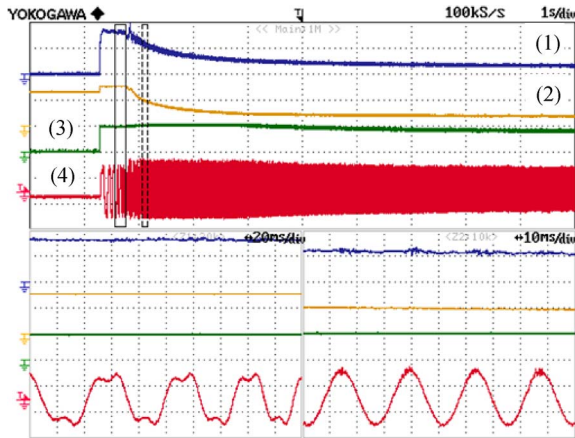


Fig. 15. Step increase in the torque from 0 to the maximum value. (1): motor torque (20 N · m/div); (2):  $i_{S1d}$  (2 A/div); (3):  $i_{S1q}$  (10 A/div); (4): stator current (10 A/div).

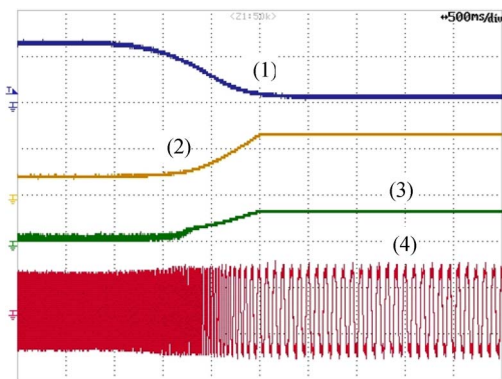


Fig. 16. Speed reduction from region III to region I. (1): motor speed (2000 r/min/div); (2):  $i_{S1d}$  (2 A/div); (3):  $i_{S3d}$  (2 A/div); (4): stator current (10 A/div).

motor is at standstill and absorbs only the magnetizing currents  $I_{Sd,rated}$ .

After the step in the torque command, the motor starts up. The line current has the maximum admissible amplitude in region I. In region II, the voltage touches the upper bound, and the control algorithm quickly reduces  $i_{S3d}$  and, accordingly,  $i_{S3q}$ , thus disabling the high-torque-density mode.

In region III, the motor flux keeps decreasing, as can be recognized by examining the waveform of  $i_{S1d}$ . It is worth noting that, in regions II and III, the control system slightly increases  $i_{S1q}$ , to entirely exploit the current limit and to take advantage of the progressive reduction of the other current components.

Fig. 15 shows the control system response under the same operating condition in Figs. 13 and 14, but focuses on regions II and III. In this transition speed range, the waveform of the line current is initially distorted due to the presence of a third harmonic component, but approaches a sinusoid as  $i_{S3d}$  decreases. Conversely, Fig. 16 shows the behavior of the machine during a deceleration from region III to region I. As can be seen, the transition between the field-weakening operation and the high-torque operation is sufficiently smooth.

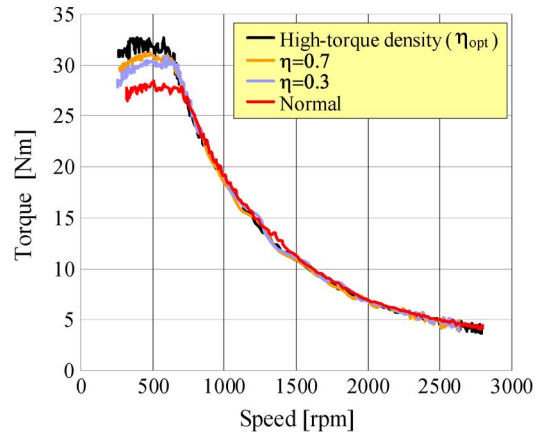


Fig. 17. Torque capability of the motor with and without high-torque-density control.

Finally, Fig. 17 compares the steady-state maximum torque that can be obtained with and without the high-torque-density control. The machine torque has been plotted versus the speed for different values of  $\eta$  when the stator current is maximum. As can be seen, the gain in the maximum torque is about 14% for  $\eta_{opt}$  compared with the case of no third harmonic injection. This result is in good agreement with the theoretical analysis. The performance of the drive for  $\eta = 0.3$  and  $\eta = 0.7$ , which are lower and greater than  $\eta_{opt}$ , respectively, is visibly worse, thus confirming the optimality of the adopted control strategy.

## VIII. CONCLUSION

In this paper, the enhancement of electromagnetic torque due to the injection of the third-order harmonic component of the magnetic field, which is possible in multiphase induction motor drives, has been analyzed under the assumption that the adsorbed stator current does not exceed the limit value. The theoretical analysis reveals that, at low torque levels, the harmonic injection does not provide any advantage, because the magnetizing current sustaining the third spatial harmonic leads to a reduction in the torque-producing current. Conversely, the improvement of the overload torque can be up to 16%–17%.

A rotor-flux-oriented control scheme capable of operating a seven-phase induction machine at its maximum possible torque at any given speed has been presented. With the exception of leakage inductance, the proposed control strategy is parameter independent and does not require the knowledge of base speed, any complex calculation of the flux level, or use of lookup tables. The feasibility of the control schemes has been verified by means of experimental tests.

## APPENDIX

The optimization problem illustrated in Section IV-A is summarized in this appendix for the sake of clarity.

The problem consists in the optimization of the motor torque, i.e.,

$$\max T_m(i_{S1d}, i_{S1q}, i_{S3d}, i_{S3q}, \eta) \quad (A1)$$

subject to the following four constraints (9), (10), (22), and (24):

- 1) ratio between third harmonic fundamental current, i.e.,

$$\eta = \frac{I_{S3d}}{I_{S1d}} \quad (\text{A2})$$

- 2) synchronization between the fundamental and third harmonic components of the air-gap field, i.e.,

$$I_{S3q} = 3 \frac{\tau_{R3}}{\tau_{R1}} \eta I_{S1q} \quad (\text{A3})$$

- 3) limited peak value of the air-gap magnetic field, i.e.,

$$C(\eta) I_{S1d} = I_{Sd, \text{rated}} \quad (\text{A4})$$

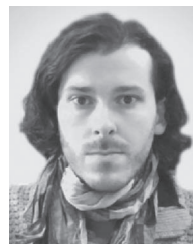
- 4) limited value of the stator current, i.e.,

$$I_{S1d}^2 + I_{S1q}^2 + I_{S3d}^2 + I_{S3q}^2 = I_S^2. \quad (\text{A5})$$

Finally, it is assumed that  $I_{Sd, \text{rated}}$  and  $I_S$  are known quantities.

## REFERENCES

- [1] E. Levi, "Multiphase electric machines for variable-speed applications," *IEEE Trans. Ind. Electron.*, vol. 55, no. 5, pp. 1893–1909, May 2008.
- [2] L. Parsa and H. A. Toliyat, "Fault-tolerant interior-permanent-magnet machines for hybrid electric vehicle applications," *IEEE Trans. Veh. Technol.*, vol. 56, no. 4, pp. 1546–1552, Jul. 2007.
- [3] W. Cao, B. C. Mecrow, G. J. Atkinson, J. W. Bennett, and D. J. Atkinson, "Overview of electric motor technologies used for More Electric Aircraft (MEA)," *IEEE Trans. Ind. Electron.*, vol. 59, no. 9, pp. 3523–3531, Sep. 2012.
- [4] A. Mohammadpour, S. Sadeghi, and L. Parsa, "A generalized fault-tolerant control strategy for five-phase PM motor drives considering star, pentagon, pentacle connections of stator windings," *IEEE Trans. Ind. Electron.*, vol. 61, no. 1, pp. 63–75, Jan. 2014.
- [5] M. Fei and R. Zanasi, "Multi-phase synchronous motors: Minimum dissipation fault-tolerant controls," in *Proc. SPEEDAM*, Sorrento, Italy, Jun. 20–22, 2012, pp. 219–224.
- [6] F. Locment, E. Semail, and X. Kestelyn, "Vectorial approach-based control of a seven-phase axial flux machine designed for fault operation," *IEEE Trans. Ind. Electron.*, vol. 55, no. 10, pp. 3682–3691, Oct. 2008.
- [7] R. Kianinezhad, B. Nahid-Mobarakeh, L. Baghli, F. Betin, and G. A. Capolino, "Modeling and control of six-phase symmetrical induction machine under fault condition due to open phases," *IEEE Trans. Ind. Electron.*, vol. 55, no. 5, pp. 1966–1977, May 2008.
- [8] A. Tani, M. Mengoni, L. Zarri, G. Serra, and D. Casadei, "Control of multiphase induction motors with an odd number of phases under open-circuit phase faults," *IEEE Trans. Power Electron.*, vol. 27, no. 2, pp. 565–577, Feb. 2012.
- [9] L. Parsa and H. A. Toliyat, "Five-phase permanent-magnet motor drives," *IEEE Trans. Ind. Appl.*, vol. 41, no. 1, pp. 30–37, Jan./Feb. 2005.
- [10] L. Parsa, N. Kim, and H. Toliyat, "Field weakening operation of a high torque density five phase permanent magnet motor drive," in *Proc. IEEE IEMDC*, May 15–18, 2005, pp. 1507–1512.
- [11] J. Wang, R. Qu, and L. Zhou, "Dual-rotor multiphase permanent magnet machine with harmonic injection to enhance torque density," *IEEE Trans. Appl. Supercond.*, vol. 22, no. 3, p. 5202204, Jun. 2012.
- [12] H. Xu, H. A. Toliyat, and L. J. Petersen, "Rotor field oriented control of five-phase induction motor with the combined fundamental and third harmonic currents," in *Proc. IEEE APEC*, 2001, pp. 392–398.
- [13] H. Xu, H. A. Toliyat, and L. J. Petersen, "Five-phase induction motor drives with DSP-based control system," *IEEE Trans. Power Electron.*, vol. 17, no. 4, pp. 524–533, Jul. 2002.
- [14] A. Abdel-Khalik, M. Masoud, and W. Barry, "Eleven-phase induction machine: Steady-state analysis and performance evaluation with harmonic injection," *IET Elect. Power Appl.*, vol. 4, no. 8, pp. 670–685, Sep. 2010.
- [15] A. S. Abdel-Khalik, S. M. Gadoue, M. I. Masoud, and B. W. Williams, "Optimum flux distribution with harmonic injection for a multiphase induction machine using genetic algorithms," *IEEE Trans. Energy Convers.*, vol. 26, no. 2, pp. 501–512, Jun. 2011.
- [16] A. S. Abdel-Khalik, M. I. Masoud, and B. W. Williams, "Improved flux pattern with third harmonic injection for multiphase induction machines," *IEEE Trans. Power Electron.*, vol. 27, no. 3, pp. 1563–1578, Mar. 2012.
- [17] A. S. Abdel-Khalik, M. I. Masoud, S. Ahmed, and A. M. Massoud, "Effect of current harmonic injection on constant rotor volume multiphase induction machine stators: A comparative study," *IEEE Trans. Ind. Appl.*, vol. 48, no. 6, pp. 2002–2013, Nov./Dec. 2012.
- [18] D. Casadei, M. Mengoni, G. Serra, A. Tani, and L. Zarri, "Torque maximization in high-torque density multiphase drives based on induction motors," in *Proc. IEEE ECCE*, Atlanta, GA, USA, Sep. 16–20, 2010, pp. 3896–3902.
- [19] L. Zarri, M. Mengoni, A. Tani, G. Serra, and D. Casadei, "Maximum-torque-per-ampere control of high torque-density multiphase drives based on induction motors," in *Proc. IEEE ECCE*, Raleigh, NC, USA, Sep. 15–20, 2012, pp. 495–502.
- [20] D. Casadei et al., "Control of a high torque density seven-phase induction motor with field-weakening capability," in *Proc. IEEE ISIE*, Bari, Italy, Jul. 4–7, 2010, pp. 2147–2152.
- [21] Ó. López, J. Álvarez, J. Doval-Gandoy, and F. D. Freijeido, "Multilevel multiphase space vector PWM algorithm," *IEEE Trans. Ind. Electron.*, vol. 55, no. 5, pp. 1933–1942, May 2008.
- [22] A. Lega, M. Mengoni, G. Serra, A. Tani, and L. Zarri, "Space vector modulation for multiphase inverters based on a space partitioning algorithm," *IEEE Trans. Ind. Electron.*, vol. 56, no. 10, pp. 4119–4131, Oct. 2009.
- [23] G. Carrasco and C. A. Silva, "Space vector PWM method for five-phase two-level VSI with minimum harmonic injection in the overmodulation region," *IEEE Trans. Ind. Electron.*, vol. 60, no. 5, pp. 2042–2205, May 2013.
- [24] J. Prieto, F. Barrero, M. J. Durán, S. Toral Marín, and M. A. Perales, "SVM procedure for n-phase VSI with low harmonic distortion in the overmodulation region," *IEEE Trans. Ind. Electron.*, vol. 61, no. 1, pp. 92–97, Jan. 2014.
- [25] N. Bodo, E. Levi, and M. Jones, "Investigation of carrier-based PWM techniques for a five-phase open-end winding drive topology," *IEEE Trans. Ind. Electron.*, vol. 60, no. 5, pp. 2054–2065, May 2013.
- [26] D. Casadei et al., "General modulation strategy for seven-phase inverters with independent control of multiple voltage space vectors," *IEEE Trans. Ind. Electron.*, vol. 55, no. 5, pp. 1921–1932, May 2008.
- [27] E. Levi, D. Dujic, M. Jones, and G. Grandi, "Analytical determination of dc-bus utilization limits in multiphase VSI supplied ac drives," *IEEE Trans. Energy Convers.*, vol. 23, no. 2, pp. 433–443, Jun. 2008.
- [28] M. Mengoni, L. Zarri, A. Tani, G. Serra, and D. Casadei, "A comparison of four robust control schemes for field-weakening operation of induction motors," *IEEE Trans. Power Electron.*, vol. 27, no. 1, pp. 307–320, Jan. 2012.
- [29] A. Abdel-Khalik, M. Daoud, S. Ahmed, A. Elserougi, and A. Massoud, "Parameter identification of five-phase induction machines with single layer windings," *IEEE Trans. Ind. Electron.*, vol. 61, no. 10, pp. 5139–5154, Oct. 2010.
- [30] H. S. Che et al., "Experimental magnetizing inductance identification in five-phase induction machines," in *Proc. IEEE IECON*, Vienna, Austria, Nov. 10–13, 2013, pp. 5179–5184.
- [31] A. G. Yepes et al., "Parameter identification of multiphase induction machines with distributed windings—Part 1: Sinusoidal excitation methods," *IEEE Trans. Energy Convers.*, vol. 27, no. 4, pp. 1056–1066, Dec. 2012.
- [32] A. Bruyere et al., "Identification of sensitive R-L parameters of a multiphase drive by a vector control," in *IEEE PESC*, Rhodes, Greece, Jun. 15–19, pp. 2523–2527.



**Michele Mengoni** (M'13) was born in Forlì, Italy, in 1981. He received the M.Sc. (Hons.) and Ph.D. degrees in electrical engineering from the University of Bologna, Bologna, Italy, in 2006 and 2010, respectively.

He is currently an Assistant Professor with the Department of Electrical, Electronic and Information Engineering "Guglielmo Marconi," University of Bologna. His research interests include the design, analysis, and control of three-phase electric machines, multiphase drives, and

ac/ac matrix converters.



**Luca Zarri** (M'05–SM'12) was born in Bologna, Italy, in 1972. He received the M.Sc. (Hons.) degree in electrical engineering and the Ph.D. degree from the University of Bologna, Bologna, in 1998 and 2007, respectively.

He was a Freelance Software Programmer from 1989 to 1992 and a Plant Designer with an engineering company from 1998 to 2002. In 2003, he became a Laboratory Engineer with the Department of Electrical, Electronic and Information Engineering "Guglielmo Marconi,"

University of Bologna, where he has been an Assistant Professor since 2005. He has authored or coauthored over 100 scientific papers. His research activity concerns the modulation strategies of power converters and the control of electric drives.

Dr. Zarri is a member of the IEEE Industry Applications, IEEE Power Electronics, and IEEE Industrial Electronics Societies.



**Angelo Tani** was born in Faenza, Italy, in 1963. He received the M.Sc. (Hons.) degree in electrical engineering from the University of Bologna, Bologna, Italy, in 1988.

In 1990, he joined the Department of Electrical Engineering, University of Bologna, where he is currently an Associate Professor. His scientific work is related to electrical machines, motor drives, and power electronics. He has authored over 100 papers published in technical journals and conference proceedings. His current

activities include multiphase motor drives, ac/ac matrix converters, and field-weakening strategies for induction motor drives.



**Leila Parsa** (S'00–M'05–SM'10) received the Ph.D. degree in electrical engineering from Texas A&M University, College Station, TX, USA.

In 2005, she joined the Department of Electrical, Computer, and Systems Engineering, Rensselaer Polytechnic Institute (RPI), Troy, NY, USA, where she is currently an Associate Professor. Her research interests are in the design, analysis, and control of electromechanical energy converters and power electronics converters for various applications.

Dr. Parsa was the recipient of the 2010 RPI School of Engineering Research Excellence Award, the 2009 Office of Naval Research Young Investigator Award, the 2007 IEEE Industry Applications Society Outstanding Young Member Award, and the 2006 IEEE Industry Applications Society Transactions Paper Award.



**Giovanni Serra** (SM'04) received the M.Sc. (Hons.) degree in electrical engineering from the University of Bologna, Bologna, Italy, in 1975.

He joined, as a recipient of a Fellowship of the National Research Council, the Department of Electrical Engineering, University of Bologna, where he became a Research Associate, has been an Associate Professor since 1987, and is currently a Professor of electrical machines.

He has authored over 180 papers published in technical journals and conference proceedings. His research interests are electrical machines, electrical drives, and power electronic converters. His current activities include multiphase drives, direct torque control of ac machines, linear motors, and ac/ac matrix converters.

Dr. Serra is a member of the IEEE Industry Applications, IEEE Dielectrics and Electrical Insulation, and IEEE Industrial Electronics Societies and the Italian Electrotechnical and Electronic Association (AEIT).



**Domenico Casadei** (SM'04–F'14) received the M.Sc. (Hons.) degree in electrical engineering from the University of Bologna, Bologna, Italy, in 1974.

Since 2001, he has been a Full Professor of electrical drives with the University of Bologna, where he served as the Head of the Department of Electrical Engineering from 2004 to 2010 and is currently the Director of the Laboratory of Electrical Machines and Drives. He has authored or coauthored over 250 papers published

in technical journals and conference proceedings. His current research interests include vector control of induction machines, multilevel converters, matrix converters, renewable energy systems, and diagnosis of electrical machines.

Dr. Casadei is a member of the IEEE Industrial Electronics and IEEE Power Electronics Societies and the European Power Electronics Society.